





Electron-impact excitation of the $(4d^{10}5s) \ ^2S_{1/2} \rightarrow (4d^95s^2) \ ^2D_{3/2}$ and $(4d^{10}5s) \ ^2S_{1/2} \rightarrow (4d^{10}6s) \ ^2S_{1/2}$ transitions in silver: Experiment and theory

B. P. Marinković , S. D. Tošić , and D. Šević 

Institute of Physics Belgrade, University of Belgrade, Pregrevica 118, 11080 Belgrade, Serbia

R. P. McEachran

Laser Physics Centre, The Research School of Physics, Australian National University, Canberra, ACT 0200, Australia

F. Blanco 

Departamento de Estructura de la Materia, Física Térmica y Electrónica e IPARCOS, Universidad Complutense de Madrid, Avienda Complutense, E-28040 Madrid, Spain

G. García

Instituto de Física Fundamental, CSIC, Serrano 113-bis, E-28006 Madrid, Spain

M. J. Brunger *

*College of Science and Engineering, Flinders University, GPO Box 2100, Adelaide, SA 5001, Australia
and Department of Actuarial Science and Applied Statistics, Faculty of Business and Management,
UCSI University, Kuala Lumpur 56000, Malaysia*



(Received 15 April 2021; accepted 22 July 2021; published 10 August 2021)

We present angle-differential and angle-integrated cross sections for electron-impact excitation of the $(4d^{10}5s) \ ^2S_{1/2} \rightarrow (4d^95s^2) \ ^2D_{3/2}$ and $(4d^{10}5s) \ ^2S_{1/2} \rightarrow (4d^{10}6s) \ ^2S_{1/2}$ transitions in atomic silver. Experimental data for four incident electron energies between 10 and 60 eV are compared with predictions from our relativistic distorted wave (RDW) and nonrelativistic atomic optical potential models. Agreement between our measured and calculated data is only fair, although in the case of the RDW it is seen to improve with increasing incident electron energy. However, only for the $(4d^{10}6s) \ ^2S_{1/2}$ excitation process, agreement of our measured data with earlier relativistic convergent close coupling results from McNamara *et al.* [*J. Phys. B* **51**, 085203 (2018)] was, with a few exceptions, typically observed to be very good, to within the uncertainties on the data.

DOI: [10.1103/PhysRevA.104.022808](https://doi.org/10.1103/PhysRevA.104.022808)

I. INTRODUCTION

Silver (Ag) is a fairly heavy atom ($Z = 47$) with, similar to the alkali metals, one valence electron (e) in an outer ($5s$) orbital leading to a $^2S_{1/2}$ ground state. It sits in the Group IB elements of the periodic table. Silver possesses high thermal and electric conductivity, and is extensively employed in various technological applications including printed circuit boards in mobile phones and computers and in conventional switches such as those used for controlling room lights. Understanding electron interactions with Ag atoms is important for improving our knowledge of laser techniques [1], in plasma diagnostics [2], astrophysics [3,4], in the development of atomic frequency standards [5,6], and most recently it may be an avenue in searching for new physics beyond the standard model [7].

It is therefore a little surprising to see the paucity of cross-section data for the e -Ag scattering system in the literature. We are aware of measurements for elastic scattering angle-

differential cross sections (DCSs) and angle-integrated cross sections (ICSSs) from Tošić *et al.* [8]. That work also included corresponding theoretical optical potential (OP) results. An initial relativistic distorted wave (RDW) computation for excitation of the $(4d^{10}5p) \ ^2P_{1/2,3/2}$ levels was reported by Zeman *et al.* [9], with subsequent experimental cross sections, although the $J = 1/2$ and $3/2$ states were not energetically resolved in their work, being given by Tošić *et al.* [10,11]. Note that in that latter work [10,11], updated RDW results from an improved code were also reported. Perhaps the most comprehensive investigation conducted so far was the relativistic convergent close coupling (RCCC) computation by McNamara *et al.* [12]. Here DCSs and ICSSs were reported for the elastic channel and eight excited electronic states of Ag, as well as for ionization [12], for incident electron energies (E_0) up to 200 eV. Nonetheless, excitation of core-excited levels, such as the energetically low-lying $(4d^95s^2) \ ^2D_{5/2}$ and $(4d^95s^2) \ ^2D_{3/2}$ states, were not considered by McNamara *et al.* [12]. To quantitatively undertake Monte Carlo simulations or multiterm Boltzmann equation modeling (see, e.g., Refs. [13–16]) of a given system, Tanaka *et al.* [17] and Brunger [18] noted that a comprehensive and complete

*Corresponding author: michael.brunger@flinders.edu.au

cross-section database is required. Therefore, we surmise that further work on e -Ag collisional behavior is required and this forms one rationale for the present investigation. A further rationale behind this study is to provide a more detailed set of experimental data, against which theory might be benchmarked. This is particularly the case for the present ($4d^{10}6s$) $^2S_{1/2}$ cross-section measurements, which are the first against which the RCCC(80) results [12] may be compared.

The structure of the remainder of this paper is as follows. In Sec. II, a description of our experimental methodology, including the uncertainties in making our measurements, is provided. The approaches we adopted to extrapolate our DCS data to 0° and 180° , in order to generate the corresponding ICS at that energy, are also described in this section. Thereafter, in Sec. III, we provide computational details of our RDW and nonrelativistic OP calculations. In Sec. IV, the current experimental and theoretical DCSs and ICSs are described and discussed, and compared to the earlier RCCC(80) results [12] where possible. Finally, some conclusions from the present investigation are given in Sec. V.

II. EXPERIMENTAL CONSIDERATIONS

In the present experimental study of some of the higher-lying excited states in Ag, we used the same spectrometer that had been specifically designed for electron–metal-atom scattering investigations [19]. It is the same spectrometer we employed in our earlier elastic scattering [8] and excitation of the unresolved ($4d^{10}5p$) $^2P_{1/2,3/2}$ levels [10,11] in silver. As a consequence, only a brief description of its utility need be given here, with an emphasis on any experimental procedures that differed from those used previously. A quasimonochromatic beam of electrons was produced through thermionic emission from a thoriated iridium filament, which in conjunction with appropriate electrostatic lenses and apertures and a hemispherical dispersion element, formed a well-focused beam at the interaction region of typical energy spread ~ 110 meV (FWHM). This electron beam was perpendicularly crossed by an atomic silver beam, that was produced by a Knudsen-type oven heated to temperatures in the range 1300–1320 K which gave rise to vapor pressures of 1.3–1.9 Pa [20]. Inelastically scattered electrons were then transported and energy analyzed by a hemispherical analyzer identical to the one in the monochromator stage, before ultimately being detected by a single channel electron multiplier.

The incident electron energies (E_0) of the present study were 10, 20, 40, and 60 eV, while the scattered electron angular range (θ) varied between 10° and 150° in 10° increments. Energy loss spectra (see Fig. 1 for a typical example) were measured at each θ , before being analyzed. For many years we calibrated, often using a variety of resonance or Wigner-cusp features for the species in question (e.g., [21–23]), our incident electron beam energy. In all that time the correction to the value of E_0 read on the relevant voltage supply was never worse than ± 0.1 eV. We therefore relied on the same calibration we employed in our recent work on indium [23] and we believe it to again be accurate to ± 0.1 eV. Note that this is something of a moot point in this case as away from the effects of resonance behavior the cross section only varies very slowly with E_0 . While McNamara *et al.* [12] did note

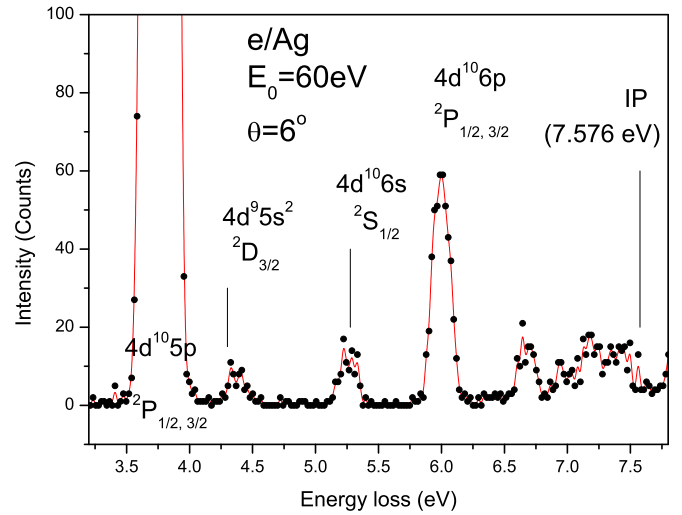


FIG. 1. Typical energy loss spectrum for electron scattering from silver. The incident electron energy was $E_0 = 60$ eV and the scattered electron angle was $\theta = 6^\circ$. Spectroscopic notation for the main features we observe is denoted on this figure. Note that the elastic peak has been suppressed for clarity, while the solid red line is simply a weighted cubic spline interpolation between the data points.

some near-threshold resonances in some of the states they investigated, those resonances were always lower in energy than the 10–60 eV energy regime of this work. The energy loss range in this investigation was from ~ 3.2 to 7.8 eV, thereby covering the whole range of the excited states up to and a little beyond the ionization threshold (see Fig. 1). Some of those states are explicitly labeled in Fig. 1, with only the lower-lying ($4d^9 5s^2$) $^2D_{5/2}$ missing as it is unresolved from the ($4d^{10}5p$) $^2P_{1/2,3/2}$ levels. Note that Tošić *et al.* [10,11] and McNamara *et al.* [12] both assumed that the contribution of the $4d_{5/2}$ state to the $5p_{1/2,3/2}$ states would be very small, and so could be ignored. The present RDW calculation (see next section), although we do not explicitly show its results, confirms the validity of that assumption. The overall energy resolution of the energy loss spectral features was ~ 160 meV (FWHM), as determined from a Gaussian fit to the isolated $4d_{3/2}$ and $6s_{1/2}$ features.

The intensity ratios for the respective areas under the ($4d^9 5s^2$) $^2D_{3/2}$ and ($4d^{10}6s$) $^2S_{1/2}$ peaks, relative to that under the unresolved ($4d^{10}5p$) $^2P_{1/2,3/2}$ peak, were determined at each θ in the range 10° – 150° and at each E_0 . From those ratios at each θ and E_0 the corresponding absolute ($4d^9 5s^2$) $^2D_{3/2}$ and ($4d^{10}6s$) $^2S_{1/2}$ DCS were simply determined by multiplying the relevant ratio by the corresponding $DCS(E_0, \theta)$ for the unresolved ($4d^{10}5p$) $^2P_{1/2,3/2}$ state from Tošić *et al.* [10,11]. The $5p_{1/2,3/2}$ DCSs of Tošić *et al.* [10,11], in the energy range 20–100 eV, were placed on an absolute scale using a generalized oscillator strength formalism [24–26], in conjunction with the known optical oscillator strength for the $5s_{1/2} \rightarrow 5p_{1/2,3/2}$ excitation [27]. At 10 eV, however, Tošić *et al.* [10,11] normalized their $5p_{1/2,3/2}$ scattered electron intensities against the corresponding RDW result at 5° . Therefore, at 10 eV, our measured $4d_{3/2}$ and $6s_{1/2}$ data are restricted to testing the shapes (angular distributions) of the corresponding RDW results, and the ratios, as a function of

TABLE I. Differential electron excitation cross sections, DCS (10^{-16} cm²/sr), and their uncertainties for the ($4d^9 5s^2$) $^2D_{3/2}$ state of Ag. The stated uncertainties are at the one standard deviation level.

Energy Scattering angle (°)	10 eV		20 eV		40 eV		60 eV	
	DCS	Uncertainty	DCS	Uncertainty	DCS	Uncertainty	DCS	Uncertainty
	(10^{-16} cm ² /sr)							
10	0.20040	0.06690	0.11319	0.04928	0.05269	0.01904	0.03745	0.01666
20	0.08280	0.04430	0.04256	0.02236	0.00625	0.00338	0.02149	0.01562
30	0.03718	0.02343	0.03795	0.02081	0.00303	0.00194	0.01583	0.01444
40	0.01351	0.00816	0.02388	0.01569	0.00256	0.00208	0.01091	0.01037
50	0.01395	0.00707	0.00423	0.00333	0.00146	0.00126	0.00197	0.00181
60	0.01188	0.00822	0.00674	0.00606	0.00165	0.00147	9.71×10^{-4}	8.44×10^{-4}
70	0.00595	0.00445	0.00332	0.00263	0.00209	0.00187	0.00132	0.00115
80	0.00497	0.00352	0.00234	0.00180	0.00269	0.00237	0.00153	0.00129
90	0.00548	0.00382	0.00517	0.00418	0.00222	0.00200	0.00166	0.00131
100	0.00497	0.00376	0.00437	0.00344	0.00424	0.00398	0.00480	0.00394
110	0.00202	0.00165	0.00360	0.00284	0.00565	0.00476	0.00843	0.00700
120	0.00181	0.00137	0.00703	0.00560	0.00512	0.00411	0.00695	0.00560
130	0.00232	0.00186	0.01092	0.00893	0.00562	0.00424	0.00570	0.00477
140	0.00681	0.00521	0.00960	0.00803	0.00866	0.00694	0.00297	0.00254
150	0.01333	0.00857	0.02154	0.01761	0.01595	0.01315	0.00156	0.00135

the scattered electron angle, of the $4d_{3/2}/5p_{1/2,3/2}$ intensities and $6s_{1/2}/5p_{1/2,3/2}$ intensities from the RDW. Note that our ratios normalization procedure is only valid if the analyser transmission remains constant across the energy-loss range 3.2–5.5 eV, at each E_0 . Our steps for ensuring this can be found, for example, in Hamilton *et al.* [23]. We should further note that McNamara *et al.* [12] raised queries as to the validity of the $5p_{1/2,3/2}$ DCSs of Tošić *et al.* [10,11]. As a result, we have reanalyzed the earlier $5p_{1/2,3/2}$ DCS data. In performing that reanalysis we found an error in the earlier work [11], which was caused at 20 and 40 eV by Tošić *et al.* incorrectly splicing their very forward-angular distributions onto their middle and backward-angular distributions. The appropriate renormalization factor to be applied to the published 20 eV $5p_{1/2,3/2}$ DCSs of Tošić *et al.* is 0.76, in reasonable accord with that suggested by McNamara *et al.* [12], while that at 40 eV is 0.42. No renormalization was needed at 10 and 60 eV, for the $5p_{1/2,3/2}$ DCSs of Tošić *et al.*, with the latter result also being consistent with that found by McNamara *et al.* [12]. A table of the corrected $5p_{1/2,3/2}$ DCSs, which we use in this work, can be obtained directly from Marinković [28], while a summary of the present ($4d^9 5s^2$) $^2D_{3/2}$ DCSs is given in Table I, and the present ($4d^{10} 6s$) $^2S_{1/2}$ DCSs are listed in Table II.

There are many factors which contribute to the overall uncertainties in cross-section measurements such as those performed here. These include uncertainties related to the electron and atomic beam stabilities throughout the measurements. Both our electron and silver beam fluxes were highly stable during the course of these experiments, with uncertainties due to their fluctuations being less than 1.5%. By far the two largest sources of uncertainty in our determination of the present DCSs were the error associated with the $5p_{1/2,3/2}$ cross sections (in the range 10%–49% depending on the actual E_0 and θ being considered), which we inherit in the normalization procedure, and the relatively small signal intensity of both the $4d_{3/2}$ (again, depending on the actual E_0 and θ being studied, the error on the $4d_{3/2}/5p_{1/2,3/2}$ ratio lay in the range

19%–66%) and $6s_{1/2}$ (the error on the $6s_{1/2}/5p_{1/2,3/2}$ ratio lay in the range 9%–67%, depending on E_0 and θ) states (see Fig. 1). When all those factors are taken into account, the overall errors on our $4d_{3/2}$ DCSs (in the range 33%–94%) can also be found in Table I, while those for the $6s_{1/2}$ state (in the range 22%–94%) are listed in Table II.

ICSs, for both the $4d_{3/2}$ and $6s_{1/2}$ states, can, at each E_0 , be derived from the corresponding DCSs. To achieve this we need to extrapolate our DCSs to 0° and 180° , perform an interpolation, and then undertake the appropriate integration. Two approaches were used to enable that aim. In the first, we took the angular dependence of the RCCC(80) results [12] to derive the $6s_{1/2}$ ICSs, while our own RDW calculations were employed to derive the $4d_{3/2}$ ICSs. In the second approach, the fitting analysis of Allen and co-workers [29,30] provided an independent self-consistency check. In all cases, the $4d_{3/2}$ and $6s_{1/2}$ ICSs we obtained, from each of the aforementioned approaches, were found to be consistent with one another to within our uncertainty estimates on the ICS. A summary of our measured ICSs and their associated uncertainties can be found in Table III. Note that our uncertainty estimates on those ICSs include all the uncertainties on the DCSs, but weighted for the $\sin \theta$ term in the integrand when calculating them, and an additional uncertainty due to the extrapolation of our DCS to 0° and 180° in order to perform the integration for each state at each E_0 .

III. THEORETICAL DETAILS

A. RDW theory

In this work the differential cross sections and integral cross sections for electron-impact excitation were calculated using the RDW method. This method was originally developed for closed-shell atoms by Zuo *et al.* [31] and then successfully applied to the heavy noble gases [32], as well as cadmium [33] and mercury [34]. It was then modified by Zeman *et al.* [35] in order to treat the electron-impact

TABLE II. Differential electron excitation cross sections, DCS (10^{-16} cm²/sr), and their uncertainties for the $(4d^{10}6s) {}^2S_{1/2}$ state of Ag. The stated uncertainties are at the one standard deviation level.

Energy	10 eV		20 eV		40 eV		60 eV	
	DCS	Uncertainty	DCS	Uncertainty	DCS	Uncertainty	DCS	Uncertainty
Scattering angle (°)	$(10^{-16}$ cm ² /sr)							
10	0.22770	0.07300	0.50650	0.11130	0.18640	0.04970	0.08800	0.03230
20	0.12040	0.06190	0.13380	0.05370	0.01810	0.00810	0.01610	0.01260
30	0.04577	0.02854	0.04818	0.02451	0.00336	0.00307	0.03800	0.02870
40	0.02110	0.01170	0.01069	0.00713	0.00766	0.00501	0.01745	0.01499
50	0.01078	0.00577	0.00501	0.00317	0.00555	0.00356	0.00592	0.00435
60	0.01088	0.00767	0.00721	0.00586	0.00824	0.00532	0.00340	0.00284
70	0.00891	0.00621	0.00408	0.00337	0.00628	0.00441	0.00158	0.00138
80	0.00456	0.00329	0.00234	0.00193	0.00592	0.00565	0.00189	0.00172
90	0.00585	0.00402	0.00409	0.00385	0.00296	0.00281	0.00181	0.00160
100	0.00538	0.00401	0.00403	0.00376	0.00660	0.00542	0.00384	0.00336
110	0.00238	0.00223	0.00499	0.00437	0.00690	0.00589	0.00763	0.00661
120	0.00326	0.00231	0.00402	0.00291	0.00717	0.00669	0.00833	0.00641
130	0.00182	0.00152	0.00286	0.00256	0.00750	0.00681	0.00505	0.00421
140	0.00386	0.00322	0.01976	0.01730	0.01444	0.01397	0.00233	0.00213
150	0.01194	0.00778	0.03525	0.02751	0.00957	0.00814	0.00222	0.00205

excitation of cesium and other alkali-metal atoms. Subsequently, this latter RDW approach was applied to the alkali-metal-like atoms silver and gold [9,36] in order to excite the resonance transitions. The reader is referred to the above papers, in particular Ref. [31], for the overall details of the RDW method.

1. Inner-shell excitation

Here the above alkali-like code was further modified to allow for the electron-impact excitation of inner-shell electrons, namely, the $(n-1)d_{3/2,5/2}$ electrons from the valence $ns_{1/2}$ shell in copper, silver, and gold; for silver we have $n=5$. In this application the ground- and excited-state wavefunctions of silver were determined in single configuration calculations using the multiconfiguration Dirac-Fock program of Grant *et al.* [37]. The distorted waves in the initial and final channels were determined by the usual procedure of electron scattering from the ground- and excited-state static potentials. These static potentials were determined in the standard manner from the ground- and excited-state Dirac-Fock orbitals of silver. The nonlocal exchange interaction was included by antisymmetrizing the total scattering wave function.

TABLE III. ICSs (10^{-16} cm²) and their uncertainties for the $(4d^9 5s^2) {}^2D_{3/2}$ and $(4d^{10} 6s) {}^2S_{1/2}$ states of Ag. The stated uncertainties are at the one standard deviation level.

Energy (eV)	$(4d^9 5s^2) {}^2D_{3/2}$		$(4d^{10} 6s) {}^2S_{1/2}$	
	ICS	Uncertainty	ICS	Uncertainty
10	0.179	0.063	0.304	0.106
20	0.159	0.026	0.326	0.114
40	0.0744	0.0261	0.163	0.057
60	0.0687	0.0241	0.130	0.045

2. Excitation of the 6s state

In this case the usual RDW code of Zeman *et al.* [35] for the alkali atoms was used. However, the ground and excited state wave functions were now determined by a polarized frozen-core model with a nonempirical polarization potential [38]. In particular, the valence orbitals were determined in the field of the Ag^+ core plus a “scaled” polarized orbital dipole potential [39]. Here the dipole polarization potential is scaled by a constant factor which is adjusted such that the energy of valence orbitals agrees with experiment. For the 5s orbital this factor was 0.97867 and for the 6s orbital it was 1.04279. A Gram-Schmidt procedure was then used to ensure the orthogonality of the 5s and 6s orbitals. Finally, the distorted waves in the initial and final channels were determined in the same manner as that given above for inner-shell excitation. Once again, the nonlocal exchange interaction was included by antisymmetrizing the total scattering wave function.

B. Atomic optical potential model

We have recently described our standard nonrelativistic optical potential approach in our studies of the electron-beryllium [40], electron-magnesium [41], electron-zinc [42], and electron-indium [43] scattering systems. The generic details of this atomic OP method were given in those papers, so only the key points of this method are summarized below.

The electron-atom interaction is described by a local complex potential given by

$$V(r) = V_s(r) + V_{ex}(r) + V_{pol}(r) + iV_{abs}(r), \quad (1)$$

where the real part comprises the following three terms. The static term V_s is derived from a Hartree-Fock calculation [44] of the atomic charge distribution. An exchange term V_{ex} accounts for the indistinguishability of the incident and target electrons; it is given by the semiclassical energy dependent formula derived by Riley and Truhlar [45]. A polarization potential V_{pol} is used for the long-range interactions which

depend on the target dipole polarizability, in the form given by Zhang *et al.* [46].

The imaginary absorption potential accounts for the electronically inelastic scattering events. It is based on the quasifree model by Staszewska *et al.* [47], but incorporates some improvements to the original formulation, such as the inclusion of screening effects, local velocity corrections, and the description of the electron indistinguishability [48] leading to a model which provides a realistic approximation for electron-atom scattering over a broad energy range [49]. We used here a standard partial wave expansion procedure. In order to obtain the l th complex partial-wave phase shift η_l , the scattering equation for the radial wave functions has been numerically integrated and the details of such a procedure can be obtained from Refs. [48,50,51]. Once the corresponding η_l phase shifts are obtained for the above potential, the elastic differential $d\sigma_{\text{elas}}/d\Omega$ and integral σ_{elas} cross sections result from the expressions

$$\frac{d\sigma_{\text{elas}}}{d\Omega} = \frac{1}{4k^2} \left| \sum_{l=0}^{l_{\text{max}}} (2l+1)(e^{2i\eta_l} - 1)P_l(\cos\theta) \right|^2 \quad (2)$$

and

$$\sigma_{\text{elas}}(E_0) = \frac{4\pi}{k^2} \sum_{l=0}^{l_{\text{max}}} (2l+1) \sin^2 \eta_l, \quad (3)$$

respectively, and the total scattering cross section (σ_{total}) results from the optical theorem $\sigma_{\text{total}}(E_0) = \frac{4\pi}{k^2} \text{Im}(f_{\theta=0})$. The total inelastic cross section $\sigma_{\text{inelas}}(E_0)$ therefore corresponds to

$$\sigma_{\text{inelas}}(E_0) = \sigma_{\text{total}}(E_0) - \sigma_{\text{elas}}(E_0). \quad (4)$$

In order to calculate the electron-impact ionization cross section, $\sigma_{\text{ion}}(E_0)$, the above calculation procedure was repeated, but using the ionization energy (IE) as the gap energy parameter, as described in Ref. [52]. In these conditions, only excitation to continuum states above the ionization threshold is considered. By combining the respective results for both gap energy parameters, summed electronic excitation cross sections (σ_{exci}) can also be derived from the expression $\sigma_{\text{exci}}(E_0) = \sigma_{\text{inelas}}(E_0) - \sigma_{\text{ion}}(E_0)$. Repeating this procedure for the threshold excitation energies, corresponding to the different excited states, their respective excitation cross sections can be extracted from the integral inelastic cross section.

While our OP calculations cannot in general compete, in terms of accuracy (except perhaps in the elastic channel [49]) and the breadth of information provided, with state-of-the-art B -spline R -matrix [53] and RCCC [12] methods, in this case no B -spline R -matrix results for electron scattering from Ag are available and the RCCC results are limited to the excitation of the $6s_{1/2}$ state. Therefore, under these circumstances, the present OP calculation results add to the story we are telling and, just as importantly, add to the available database for this scattering system.

IV. RESULTS AND DISCUSSION

In Table I and Figs. 2(a)–2(d), we present our measured ($4d^9 5s^2$) $^2D_{3/2}$ excitation DCSs for the incident electron energies (a) 10 eV, (b) 20 eV, (c) 40 eV, and (d) 60 eV. Also shown in Fig. 2 are the corresponding results from our current RDW

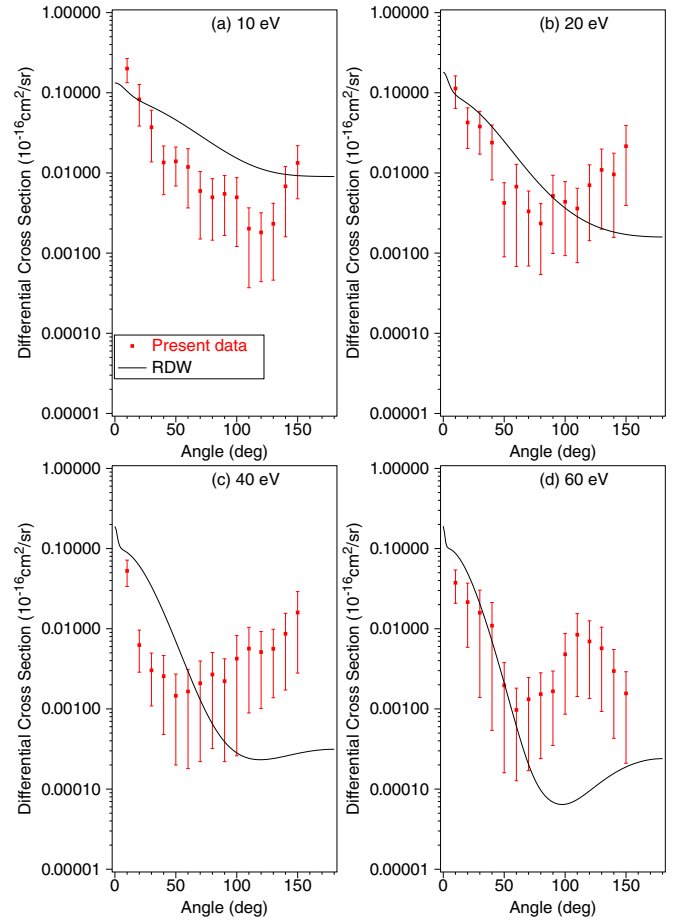


FIG. 2. Differential cross sections ($\times 10^{-16}$ cm²/sr) for electron-impact excitation of the ($4d^9 5s^2$) $^2D_{3/2}$ state of silver. The present data (■) are compared against theoretical results from our RDW calculations (—).

computations. There are several general observations we can make with regard to Fig. 2. Firstly, it is clear that there are no other experimental or theoretical data currently available in the literature to compare against. In particular, we note that McNamara *et al.* [12] did not consider any core-excited processes in their otherwise detailed study of Ag. Thus our results for this excitation process are unique. The second point we can glean from Fig. 2 is that the agreement between our measured DCS and RDW computed DCS, at each E_0 , is only fair. This level of accord probably improves somewhat as the incident electron energy is increased, as one might anticipate with the RDW method, but a more quantitative description is difficult here given the measurement uncertainties. Inner-shell quadrupole transitions present a real challenge to theory, so that in the present application more elaborate (multiconfiguration) wave functions will probably be needed in order to better describe the collision dynamics of this excitation process. Finally, with the possible exception of the 60-eV experimental angular distribution, we note that both our measured and calculated ($4d^9 5s^2$) $^2D_{3/2}$ differential cross sections display little or no angular structure. As we shall shortly see, this is in marked contrast to the angular distributions for excitation of the ($4d^{10} 6s$) $^2S_{1/2}$ state. Note that as the $4d_{3/2}$ quadrupole

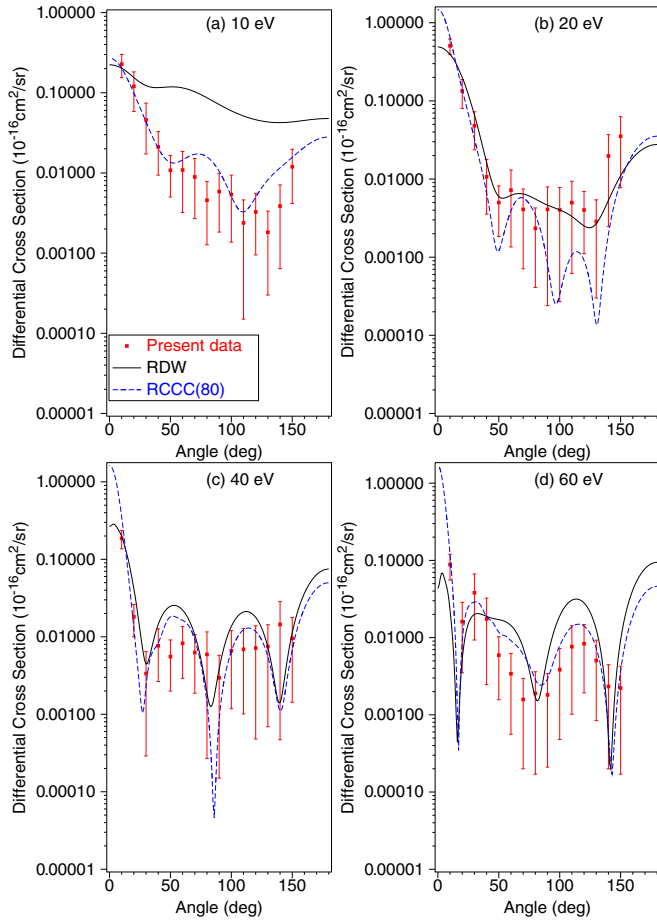


FIG. 3. Differential cross sections ($\times 10^{-16}$ cm²/sr) for electron-impact excitation of the $(4d^{10}6s)^2S_{1/2}$ state of silver. The present data (■) are compared against theoretical results from our RDW calculations (—) and the RCCC(80) computations of McNamara *et al.* [12] (---).

transition is very weak compared to the $6s_{1/2}$ excitation and, in particular, the unresolved $5p_{1/2,3/2}$ transitions, it is likely that only very few of the initial partial waves are important in describing that quadrupole transition. Consequently, the “interference” effects between the partial waves are reduced so that the $4d_{3/2}$ angular distribution exhibits less structure.

In Table II and Figs. 3(a)–3(d) we present our measured $(4d^{10}6s)^2S_{1/2}$ excitation DCSs, again for the incident electron energies (a) 10 eV, (b) 20 eV, (c) 40 eV, and (d) 60 eV. Also shown in Fig. 3 are the corresponding results from our RDW computation and the RCCC(80) calculation of McNamara *et al.* [12]. Agreement between the present measured DCSs and the RCCC(80) results [12] is seen to be very good, in terms of both the shapes and absolute cross-section values, at each E_0 studied. This provides further evidence for the efficacy of the RCCC(80) theory to be used as a good starting point to construct a complete database for Ag in modeling applications of its behavior in low-temperature plasmas and gaseous electronics in general. On the other hand, the comparison between our present measured and RDW calculated DCSs is not as impressive as that just described. Nonetheless, the RDW does improve, certainly in terms of the shapes of

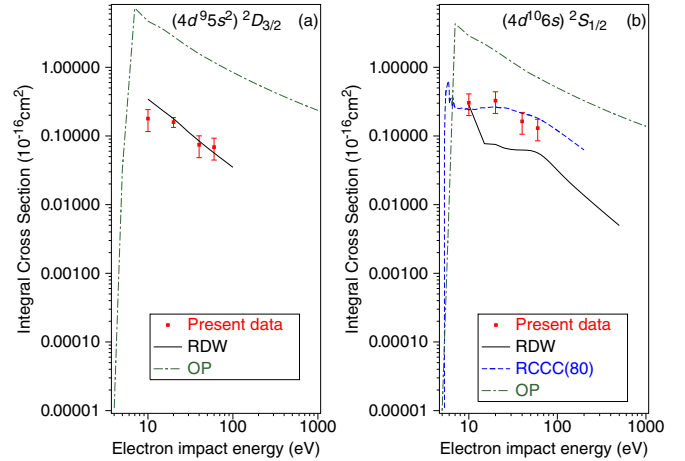


FIG. 4. Integral cross sections ($\times 10^{-16}$ cm²) for electron-impact excitation of the (a) $(4d^9 5s^2)^2D_{3/2}$ and (b) $(4d^{10}6s)^2S_{1/2}$ states of silver. The present data (■) are compared against theoretical results from our RDW calculations (—), OP calculations (---), and the RCCC(80) computations of McNamara *et al.* [12] (---).

the $6s_{1/2}$ angular distributions and their magnitude, as E_0 is increased. One of the key features from the present study is the strong oscillatory nature of the $(4d^{10}6s)^2S_{1/2}$ angular distributions in Fig. 3. Indeed this behavior appears to be ubiquitous in electron-metal-vapor scattering, for both the elastic and discrete inelastic channels, with a few examples supporting that assertion being bismuth [22], zinc [21], indium [23], sodium [54], and magnesium [55]. The oscillatory nature of any differential cross section arises from the interference between the various partial waves that describe the collisional behavior. In the present case of inelastic scattering, the details depend in a complex way on the interference between T -matrix elements that need to be combined with spherical harmonics in order to generate the scattering amplitudes [56] and, subsequently, the angle-differential cross section [57]. It is, therefore, generally not possible to predict either the number or the positions of the minima (maxima) in the DCS. Even though in some special circumstances and models a resemblance to elastic scattering may appear in inelastic collisions [58], and the DCS generally exhibits less structure in the angular dependence with decreasing projectile energy, drawing truly quantitative conclusions is not possible.

In Table III and Figs. 4(a) and 4(b), we present our respective derived $4d_{3/2}$ and $6s_{1/2}$ experimental excitation ICSs. Also shown, where possible, in Fig. 4 are the corresponding results from our RDW and OP calculations, and those from the RCCC(80) computation of McNamara *et al.* [12]. Considering first the $4d_{3/2}$ state [see Fig. 4(a)], we find that with the exception of the 10 eV ICS, there is a very good level of agreement between our measured and RDW calculated ICSs. Given our previous discussion, for the excitation of the $4d_{3/2}$ level at the DCS level, that degree of accord can only be due to a happy cancellation of divergences in the integrand, coupled with roughly the same theory and experimental DCS magnitudes, and so must be considered to be somewhat fortuitous. Our atomic OP calculation clearly overestimates the magnitude of the experimental ICSs over the entire 10–60 eV energy

range. However, the functional dependence (shape) of our OP integral cross section corresponds quite well with that of the experimental data, so that an appropriately scaled OP ICS might be used, in the context of assembling a complete Ag database, to extend the measured cross sections to larger energies and down to threshold. For the $6s_{1/2}$ ICSs [see Fig. 4(b) and Table III], we find a very good level of accord between our measured cross sections and those calculated within the RCCC(80) approach [12]. Furthermore, that statement holds across the entire common energy range. Figure 4(b) also clearly indicates that our RDW ICS typically underestimates the magnitude of the measured data, between 20 and 60 eV, which, even allowing for the $\sin \theta$ term in the integrand, probably reflects its inability to describe the very forward angle DCSs which are strongly peaked at small scattering angles (see Fig. 3). Finally, we note that our present atomic optical potential ICS overestimates significantly the magnitude of the $6s_{1/2}$ experimental ICS [see Fig. 4(b)]. This result, and that for the $4d_{3/2}$ state, reflect difficulties in our semiphenomenological approach to extracting individual integral excitation cross sections from the total inelastic cross section that is calculated *ab initio*.

V. CONCLUSIONS

We have reported on experimental and theoretical DCS and ICS results for electron-impact excitation of the $(4d^{10}5s) \ ^2S_{1/2} \rightarrow (4d^95s^2) \ ^2D_{3/2}$ and $(4d^{10}5s) \ ^2S_{1/2} \rightarrow (4d^{10}6s) \ ^2S_{1/2}$ transitions in silver, and in doing so we have extended the available cross-section database for this scattering system. Neither of those transitions are electric-dipole allowed, so that the corresponding measured scattering intensities were relatively low which in turn led to higher statistical uncertainties than were normally found to be the case [10,11,23]. Nonetheless, all our measured data were observed to be consistently reproducible, to within the stated one standard deviation uncertainties, so that we are confident in their validity.

For the excitation of the $(4d^95s^2) \ ^2D_{3/2}$ state, at the DCS level only the present RDW calculation could be compared to our experimental data. Here the level of accord between them was found to be only fair, with more elaborate (multiconfiguration) wave functions probably being required to improve

our description of this inner-shell quadrupole transition. At the ICS level, however, our RDW and OP computations could now be compared to our data. Here the OP calculation was found to overestimate the magnitude of the ICS across the common energy range, although its energy dependence was in good qualitative accord with our measurements. The excellent agreement between our RDW calculation and experimental data, across 20–60 eV, was undoubtedly somewhat fortuitous given the behavior at the DCS level.

For the excitation of the $(4d^{10}6s) \ ^2S_{1/2}$ state, a very good level of accord was found between our measured DCSs and the RCCC(80) calculated DCSs at all common incident electron energies. For this state the RDW computation also provided a fair description for this scattering process, with the level of accord between our measured and calculated DCS improving as E_0 increased. This was no real surprise, as based on our experience the RDW method becomes quite reliable above two to three times the ionization energy of the target in question (for silver the ionization energy = 7.576 eV). Strong interference effects, both constructive and destructive, in the partial waves describing the $5s \rightarrow 6s$ scattering process were clearly observed in our measured and calculated angular distributions, as was their energy dependence. Finally, we note the excellent agreement between our measured ICS and the RCCC(80) ICS for this transition. Agreement with our RDW and OP ICS was found to be less satisfactory, although the qualitative energy dependence of the OP calculation was again in good accord with the experimental ICS.

ACKNOWLEDGMENTS

This work was financially supported, in part, by the Australian Research Council (Project No. DP180101655), the Institute of Physics Belgrade through the Ministry of Education, Science and Technological Development (MESTD) of Serbia, and the Spanish Ministerio de Ciencia e Innovación - MICNN (Project No. PID2019–104727RB-C21) and CSIC (Project No. LINKA 20085). We thank Dr. L. Campbell for his help with some aspects of this paper, and Professor D. V. Fursa for providing us with tables of his RCCC(80) results. R.P.M. acknowledges very valuable discussions with Professor A. D. Stauffer in the early stages of the development of the inner-shell RDW method.

-
- [1] B. Wernsman, T. Prabhuran, K. Lewis, F. Gonzales, M. Villagran, and J. J. Rocca, *IEEE J. Quantum Electron.* **24**, 1554 (1988).
 - [2] P. Choi and M. B. Favre, *J. Phys. D* **20**, 169 (1987).
 - [3] J. A. Johnson and M. Boltz, *Astrophys. J.* **579**, 616 (2002).
 - [4] D. Kasen, B. Metzger, J. Barnes, E. Quataert, and E. Ramirez-Ruiz, *Nature (London)* **551**, 80 (2017).
 - [5] G. Uhlenberg, J. Dirscherl, and H. Walther, *Phys. Rev. A* **62**, 063404 (2000).
 - [6] T. Badr, M. D. Plimmer, P. Juncar, M. E. Himbert, Y. Louyer, and D. J. E. Knight, *Phys. Rev. A* **74**, 062509 (2006).
 - [7] V. A. Dzuba, S. O. Allehabi, V. V. Flambaum, J. Li, and S. Schiller, *Phys. Rev. A* **103**, 022822 (2021).
 - [8] S. D. Tošić, V. I. Kelemen, D. Šević, V. Pejčev, D. M. Filipović, E. Yu. Remeta, and B. P. Marinković, *Nucl. Instrum. Methods B* **267**, 283 (2009).
 - [9] V. Zeman, R. P. McEachran, and A. D. Stauffer, *Can. J. Phys.* **74**, 889 (1996).
 - [10] S. D. Tošić, V. Pejčev, D. Šević, R. P. McEachran, A. D. Stauffer, and B. P. Marinković, *Nucl. Instrum. Methods B* **279**, 53 (2012).
 - [11] S. D. Tošić, V. Pejčev, D. Šević, R. P. McEachran, A. D. Stauffer, and B. P. Marinković, *Phys. Rev. A* **91**, 052703 (2015).

- [12] K. McNamara, D. V. Fursa, and I. Bray, *J. Phys. B* **51**, 085203 (2018).
- [13] A. I. Lozano, K. Krupa, F. Ferreira da Silva, P. Limão-Vieira, F. Blanco, A. Munõz, D. B. Jones, M. J. Brunger, and G. García, *Eur. Phys. J. D* **71**, 226 (2017).
- [14] F. Costa, A. Traoré-Dubuis, L. Álvarez, A. I. Lozano, X. Ren, A. Dorn, P. Limão-Vieira, F. Blanco, J. C. Oller, A. Muñoz, A. García-Abenza, J. D. Gorfinkiel, A. S. Barbosa, M. H. F. Bettega, P. Stokes, R. D. White, D. B. Jones, M. J. Brunger, and G. García, *Int. J. Mol. Sci.* **21**, 6947 (2020).
- [15] P. W. Stokes, M. J. E. Casey, D. G. Cocks, J. de Urquijo, G. García, M. J. Brunger, and R. D. White, *Plasma Sources Sci. Technol.* **29**, 105008 (2020).
- [16] P. W. Stokes, S. P. Foster, M. J. E. Casey, D. G. Cocks, O. González-Magaña, J. D. Urquijo, G. García, M. J. Brunger, and R. D. White, *J. Chem. Phys.* **154**, 084306 (2021).
- [17] H. Tanaka, M. J. Brunger, L. Campbell, H. Kato, M. Hoshino, and A. R. P. Rau, *Rev. Mod. Phys.* **88**, 025004 (2016).
- [18] M. J. Brunger, *Int. Rev. Phys. Chem.* **36**, 333 (2017).
- [19] B. P. Marinković, V. Pejčev, D. M. Filipović, D. Šević, S. Milisavljević, and B. Predojević, *Radiat. Phys. Chem.* **76**, 455 (2007).
- [20] C. B. Alcock, V. P. Itkin, and M. Y. Harrigan, *Can. Metall. Q.* **23**, 309 (1984).
- [21] B. P. Marinković, R. Panajotović, D. Šević, R. P. McEachran, G. García, F. Blanco, and M. J. Brunger, *Phys. Rev. A* **99**, 062702 (2019).
- [22] B. Predojević, D. Šević, B. P. Marinković, R. P. McEachran, F. Blanco, G. García, and M. J. Brunger, *Phys. Rev. A* **101**, 032704 (2020).
- [23] K. R. Hamilton, O. Zatsarinny, K. Bartschat, M. S. Rabasović, D. Šević, B. P. Marinković, S. Dujko, J. Atić, D. V. Fursa, I. Bray, R. P. McEachran, F. Blanco, G. García, P. W. Stokes, R. D. White, and M. J. Brunger, *Phys. Rev. A* **102**, 022801 (2020).
- [24] E. N. Lassetre, *J. Chem. Phys.* **43**, 4479 (1965).
- [25] L. Vriens, *Phys. Rev.* **160**, 100 (1967).
- [26] H. Kato, H. Kawahara, M. Hoshino, H. Tanaka, M. J. Brunger, and Y.-K. Kim, *J. Chem. Phys.* **126**, 064307 (2007).
- [27] J. R. Fuhr and W. L. Wiese, in *CRC Handbook of Chemistry and Physics*, 89th ed., edited by D. R. Lide (CRC, Boca Raton, FL, 2009).
- [28] bratislav.marinkovic@ipb.ac.rs.
- [29] L. J. Allen, M. J. Brunger, I. E. McCarthy, and P. J. O. Teubner, *J. Phys. B* **20**, 4861 (1987).
- [30] M. J. Brunger, S. J. Buckman, L. J. Allen, I. E. McCarthy, and K. Ratnavelu, *J. Phys. B* **25**, 1823 (1992).
- [31] T. Zuo, R. P. McEachran, and A. D. Stauffer, *J. Phys. B* **24**, 2853 (1991).
- [32] T. Zuo, R. P. McEachran, and A. D. Stauffer, *J. Phys. B* **25**, 3393 (1992).
- [33] R. Srivastava, T. Zuo, R. P. McEachran, and A. D. Stauffer, *J. Phys. B* **25**, 1073 (1992).
- [34] R. Srivastava, T. Zuo, R. P. McEachran, and A. D. Stauffer, *J. Phys. B* **25**, 2409 (1992).
- [35] V. Zeman, R. P. McEachran, and A. D. Stauffer, *J. Phys. B* **27**, 3175 (1994).
- [36] M. Maslov, M. J. Brunger, P. J. O. Teubner, O. Zatsarinny, K. Bartschat, D. V. Fursa, I. Bray, and R. P. McEachran, *Phys. Rev. A* **77**, 062711 (2008).
- [37] I. P. Grant, B. J. McKenzie, P. H. Norrington, D. F. Mayer, and N. C. Pyper, *Comput. Phys. Commun.* **21**, 207 (1980).
- [38] R. P. McEachran and M. Cohen, *J. Phys. B* **16**, 3125 (1983).
- [39] R. P. McEachran, D. L. Morgan, A. G. Ryman, and A. D. Stauffer, *J. Phys. B* **10**, 663 (1977).
- [40] R. P. McEachran, F. Blanco, G. García, and M. J. Brunger, *J. Phys. Chem. Ref. Data* **47**, 033103 (2018).
- [41] R. P. McEachran, F. Blanco, G. García, P. W. Stokes, R. D. White, and M. J. Brunger, *J. Phys. Chem. Ref. Data* **47**, 043104 (2018).
- [42] R. P. McEachran, B. P. Marinković, G. García, R. D. White, P. W. Stokes, D. B. Jones, and M. J. Brunger, *J. Phys. Chem. Ref. Data* **49**, 013102 (2020).
- [43] K. R. Hamilton, O. Zatsarinny, K. Bartschat, M. S. Rabasović, D. Šević, B. P. Marinković, S. Dujko, J. Atić, D. V. Fursa, I. Bray, R. P. McEachran, F. Blanco, G. García, P. W. Stokes, R. D. White, D. B. Jones, L. Campbell, and M. J. Brunger, *J. Phys. Chem. Ref. Data* **50**, 013101 (2021).
- [44] R. D. Cowan, *The Theory of Atomic Structure and Spectra* (University of California Press, Berkeley, 1981).
- [45] M. E. Riley and D. G. Truhlar, *J. Chem. Phys.* **63**, 2182 (1975).
- [46] X. Zhang, J. Sun, and Y. Liu, *J. Phys. B* **25**, 1893 (1992).
- [47] G. Staszewska, D. W. Schwenke, D. Thirumalai, and D. G. Truhlar, *Phys. Rev. A* **28**, 2740 (1983).
- [48] F. Blanco and G. García, *Phys. Rev. A* **67**, 022701 (2003).
- [49] O. Zatsarinny, K. Bartschat, G. García, F. Blanco, L. R. Hargreaves, D. B. Jones, R. Murrie, J. R. Brunton, M. J. Brunger, M. Hoshino, and S. J. Buckman, *Phys. Rev. A* **83**, 042702 (2011).
- [50] F. Blanco and G. García, *Phys. Lett. A* **255**, 147 (1999).
- [51] F. Blanco and G. García, *Phys. Lett. A* **295**, 178 (2002).
- [52] L. Chiari, A. Zecca, G. García, F. Blanco, and M. J. Brunger, *J. Phys. B* **46**, 235202 (2013).
- [53] O. Zatsarinny and K. Bartschat, *Phys. Rev. A* **79**, 042713 (2009).
- [54] P. J. O. Teubner, J. L. Riley, M. J. Brunger, and S. J. Buckman, *J. Phys. B* **19**, 3313 (1986).
- [55] M. J. Brunger, J. L. Riley, R. E. Scholten, and P. J. O. Teubner, *J. Phys. B* **21**, 1639 (1988).
- [56] K. Bartschat and N. S. Scott, *Comput. Phys. Commun.* **30**, 369 (1983).
- [57] K. Bartschat, *Comput. Phys. Commun.* **30**, 383 (1983).
- [58] C. K. Bartschat and K. Blum, *J. Phys. B* **15**, 2747 (1982).